HHS Public Access

Author manuscript

Eur Radiol. Author manuscript; available in PMC 2016 October 01.

Published in final edited form as:

Eur Radiol. 2015 October ; 25(10): 2840–2850. doi:10.1007/s00330-015-3701-8.

Haralick Texture Analysis of prostate MRI: Utility for differentiating non-cancerous prostate from prostate cancer and differentiating prostate cancers with different Gleason Scores

Andreas Wibmer, MD[1], **Hedvig Hricak, MD**[1], **Tatsuo Gondo, MD**[2], **Kazuhiro Matsumoto, MD**[2], **Harini Veeraraghavan, PhD**[3], **Duc Fehr, PhD**[3], **Junting Zheng**[4], **Debra Goldman**[4], **Chaya Moskowitz, PhD**[4], **Samson Fine, MD**[5], **Victor E. Reuter, MD**[5], **James Eastham, MD**[2], **Evis Sala, MD**[1], and **Hebert Alberto Vargas, MD**[1]

[1]Memorial Sloan Kettering Cancer Center, Department of Radiology, 1275 York Avenue, 10065 New York City, NY, United States

[2]Memorial Sloan Kettering Cancer Center, Department of Urology, 1275 York Avenue, 10065 New York City, NY, United States

[3]Memorial Sloan Kettering Cancer Center, Department of Medical Physics, 1275 York Avenue, 10065 New York City, NY, United States

[4]Memorial Sloan Kettering Cancer Center, Department of Epidemiology and Biostatistics, 1275 York Avenue, 10065 New York City, NY, United States

[5]Memorial Sloan Kettering Cancer Center, Department of Pathology, 1275 York Avenue, 10065 New York City, NY, United States

Abstract

Objectives—To investigate Haralick texture analysis of prostate MRI for cancer detection and differentiating Gleason Scores (GS).

Methods—One hundred and forty-seven patients underwent T2- weighted (T2WI) and diffusion-weighted prostate MRI. Cancers ≥0.5ml and non-cancerous peripheral (PZ) and transition zone (TZ) tissue were identified on T2WI and apparent diffusion coefficient (ADC) maps, using whole-mount pathology as reference. Texture features (Energy, Entropy, Correlation, Homogeneity, Inertia) were extracted and analyzed using generalized estimating equations.

Results—PZ cancers (n=143) showed higher Entropy and Inertia and lower Energy, Correlation and Homogeneity compared to non-cancerous tissue on T2WI and ADC maps (p-values: <.0001–0.008). In TZ cancers (n=43), we observed significant differences for all five texture features on the ADC map (all p-values: <.0001) and for Correlation (p=0.041) and Inertia (p=0.001) on T2WI. On ADC maps, GS was associated with higher Entropy (GS 6 vs 7: p=0.0225; 6 vs >7: p=0.0069) and lower Energy (GS 6 vs 7: p=0.0116, 6 vs >7: p=0.0039). ADC map Energy (p=0.0102) and

Corresponding Author and requests for reprints: Andreas Wibmer, MD, Memorial Sloan Kettering Cancer Center, Department of Radiology, 1275 York Avenue; 10065 New York City, NY, Tel.: (212) 639 3116; Fax.: (212) 717 3658, a.wibmer@gmx.net.

Disclosure:
There were no sources of support or conflicts of interest which require disclosure.

Entropy (p=0.0019) were significantly different in GS ≤3+4 vs. ≥4+3 cancers; ADC map Entropy remained significant after controlling for the median ADC (p=0.0291).

Conclusion—Several Haralick based texture features appear useful for prostate cancer detection and GS assessment.

Keywords

Prostatic Neoplasm; Adenocarcinoma; Magnetic Resonance Imaging; Image Processing; Computer-Assisted; Gleason Grading

INTRODUCTION

There is increasing interest in the potential role of magnetic resonance imaging (MRI) for evaluating prostate cancer aggressiveness, capable of allowing a risk-adjusted management approach [1; 2]. Patients with low-volume low-grade (i.e. Gleason score 3+3=6) cancers may be offered conservative management with strategies such as active surveillance, while patients with high-risk of progression or death from prostate cancer are treated with more radical approaches such as surgery or radiation therapy [3–6]. This risk-based management paradigm is heavily dependent on adequate patient selection, and it is well known that standard risk-stratification methods based on physical exam, serum prostate-specific antigen (PSA) testing and transrectal prostate biopsy are far from optimal [7].

According to European Society of Urogenital Radiology prostate MRI guidelines [8], muliparametric (mp)-MRI combines anatomical T1- and T2-weighted sequences with at least two “functional” sequences such as diffusion-weighted (DW) MRI, dynamic contrast-enhanced MRI and/or magnetic resonance spectroscopy. Significant associations between several quantitative parameters derived from mp-MRI and prostate tumour aggressiveness have been reported. Tumour-to-muscle signal intensity ratios on T2-weighted images (T2WI) and apparent diffusion coefficients (ADC) on DW-MRI have been found to be negatively correlated to tumor Gleason score on pathology [9–16]. The discriminatory abilities of these parameters are only moderate due to considerable overlaps between different Gleason scores. This, and technical variations in MRI acquisition (e.g. different scanner systems, different b-values) challenge the translation of these findings to clinical practice. Moreover, there is debate about the methodology and reproducibility of ADC measurements with the recent description of ADC ratios (normalized to non-tumorous tissues) [17], whole lesion measurement and histogram analysis including median and low percentile ADC values [18]. More advanced methods of image processing and analysis may be a next step to overcome this limitation.

Haralick texture analysis is a mathematical method that extracts features from an image that are not perceptible for the human eye [19]. In essence, it describes how often one grey tone will appear in a specified spatial relationship to another gray tone on the image [20]. By using a series of mathematical equations, it generates a range of quantitative parameters (‘texture features’) that characterize the spatial variation of gray levels throughout an image. Successful applications of this technique have been documented in a variety of fields [19; 21; 22]. We therefore hypothesized that this image analysis technique could also be applied

in mp-MRI of the prostate and could potentially support diagnosis, risk stratification and management-decisions in prostate cancer.

The purpose of this proof of principle study was to investigate whether Haralick texture analysis of prostate MRI is useful for prostate cancer detection and differentiating cancers with different Gleason Scores (GS).

MATERIALS AND METHODS

The Institutional Review Board approved this retrospective study and waived written informed consent.

Study population

The following inclusion criteria were queried from our electronic hospital information system: (1) biopsy-proven prostate cancer; (2) radical prostatectomy performed in our institution between January-December 2011; (3) endorectal 3T prostate MRI performed within six months before prostatectomy and (4) whole-mount step-section pathologic tumour maps. Patients with (1) previous treatment for prostate cancer (i.e. radiation or hormonal therapy, n=7), (2) those who had imaging artefacts making the segmentation of cancer lesions impossible (n=8), (3) those where the size and/or the location of the cancer lesions precluded the segmentation of non-cancerous prostate tissue (n=4), and (4) those with a total tumour volume <0.5ml on histopathology (n=51), were excluded from the analysis. Figure 1 is a flow chart that details the patient selection.

MR Imaging Acquisition

All images were acquired on a 3.0-T MRI system (Signa, General Electric Medical Systems, Milwaukee, USA). A pelvic phased-array coil was used in combination with an endorectal coil (Medrad, Warrendale, USA) for signal reception. Transverse T1-weighted images were acquired as follows: repetition time/echo time (msec), 467–1349/6.6–10.2; section thickness, 5mm; intersection gap, 1mm; field of view, 22–40cm; and matrix, 256×192 to 448×224. Transverse, coronal, and sagittal T2-weighted fast spin-echo images were acquired as follows: repetition time/echo time (msec) 2500–7700/83.3–143.5; section thickness, 3–4mm; intersection gap, 0–1mm; field of view, 14–24cm; and matrix, 288×288 to 448×224. Transverse DW sequences were acquired with a single-shot spin-echo echo-planar imaging sequence with two *b* values (0 and 1000 sec/mm^2) (3500–5675/70.3–105.6; section thickness, 3–4mm; no intersection gap; field of view, 14–24cm; matrix, 96×96 to 128×128) and with the same orientation and location used to acquire transverse T2-weighted images. ADC maps were calculated using a designated workstation (Advanced Workstation; General Electric Medical Systems).

Histopathologic Analysis and Pathologic Volume Measurement

All radical prostatectomy specimens were serially sectioned from apex to base at 3–5 mm intervals, and submitted as whole-mount sections for examination. After detailed microscopic revision, the tumour border was outlined on the coverslip of each slide, and the Gleason grade patterns present in each lesion were determined. Then radical prostatectomy

slides were scanned as 300-dpi resolution digitalized tumour maps. Tumour volume for each cancer focus was calculated by multiplying the tumour area by the slice thickness with computerized planimetry using image analysis and measurement software Photoshop CS6 (Adobe Systems, San Jose, CA, USA).

Image Segmentation

Segmentation of prostate cancer foci and non-cancerous prostate tissue on the MR images was done in consensus by three readers: one genitourinary imaging research fellow (A.W.), one clinical urology research fellow (T.G.), and one pathology research fellow (K.M.), using a designated multi-platform, free and open source software package for visualization and medical image computing (3D slicer, version 4.2.2–1; available at: http://slicer.org/). Prostate cancer foci ≥0.5ml were first identified on the whole-mount step-section tumour maps. Then, using anatomical landmarks (e.g. urethra, ejaculatory ducts, well-delineated hyperplastic nodules, prostatic capsule) as a reference for visual co-registration, freehand regions of interest were drawn on the T2WI and ADC maps, matching the location of tumours on the whole-mount pathology maps (Figure 2). If a lesion extended into more than one histopathologic slice, the tumour was segmentated on every corresponding MR image creating a volume of interest (VOI). In every patient, one separate VOI was placed in a region of non-cancerous peripheral and transition zone prostate tissue according to histopathology, avoiding nodules of benign prostate hyperplasia.

Texture Analysis

Textural features were extracted from the MR images using Haralick texture descriptors. These features are computed from the grey level co-occurrence matrices (GLCM) computed at each voxel underlying the region of interest in the 3D volume [19]. The GLCM is essentially a two dimensional histogram that captures the frequency of co-occurrence of two pixel intensities at a certain offset with respect to each other over the region where the texture is computed (Figure 3). In the original work in [19], 28 different features were used. The work in [23] eliminated redundant features and reduced the number of required texture features to seven. These features are Energy, Entropy, Correlation, Difference Moment or Homogeneity, Inertia or Contrast, Cluster Shade, and Cluster Prominence. Each texture feature computes a specific relation of pixels with their local neighbourhood, as detailed in Table 1. Cluster Shade and Cluster Prominence were not calculated in this study because these features tend to over emphasize Energy, Entropy, Homogeneity and Contrast. The texture features were computed over the whole volume defined by the segmentation mask for a structure. The result of texture analysis on a structure is a set of scalar (single unit) values that summarize the texture in that region. It is important to highlight that Haralick analysis is only one of multiple techniques that can be used to generate “texture” data. Another such technique is fractal based texture analysis [24], which examines the difference between pixels at different scales (offset distances) and then estimates a stochastic model. Our preference for Haralick analysis is based on the following reasons. First, fractal based texture models are computationally intensive as the model is estimated during the texture extraction process. Second, these models lack orientation sensitivity and are not suitable for describing local image structures. We computed the texture features over the whole volume defined by the segmentation mask for a structure, as has been previously done in medical

studies for characterizing heterogeneity of tumours [25; 26], rather than spatially local textures. The main difference between these two methods is that in the volume-based approach a single value is returned for the entire volume for each texture feature as opposed to a separate texture feature value for each pixel. An advantage of the volume-based approach is that it is not impacted by the choice of spatial granularity or the radius over which a texture is computed. This measure is therefore more robust to the size of the tumour, albeit for very small tumour sizes, the measure can be adversely affected by noise in the same way as local textures. The texture analysis was performed separately on the T2WI and ADC images, wherein, the images were first normalized and rescaled to an intensity range of 0–256 gray levels followed by texture analysis. The GLCM was computed by using 128 bins, and employing image offsets in all the 24 directions (for 2D it is 8 directions as there are 8 neighbours for a voxel and 24 for 3D) followed by averaging of the offset values from all the directions. Using multiple offsets enabled the method to be rotationally invariant to the distribution of texture. The texture features were computed using an in-house software written in C++ together with the publicly available Insight ToolKit (ITK) software libraries for image analysis [27]. The ITK software libraries provide application interface (API) tools for reading DICOM images, performing various image preprocessing on radiological images as well as methods for computing texture features. The software was written and tested on a 16-core Windows7 PC. The libraries needed to compile the software include Visual studio 2012, Insight ToolKit Software Development Kit, and CMake [28].

Statistical methods

MRI texture parameters were summarized using descriptive statistics. Scatter plots were used to show texture parameter value of every cancer lesion by the value of non-cancerous tissue from the same patient. The difference of parameter values between cancer lesion and non-cancerous tissue was calculated and tested using the generalized estimating equations (GEE) method with a robust covariance matrix and independent correlation structure to take into account multiple tissue samples per patients. Box and whisker plots were used to plot each texture parameter in tumours by Gleason score.

Generalized linear regression and the GEE method was used to examine the association between texture parameters and tumour Gleason score. Custom hypothesis tests were created to test the difference between Gleason scores of 3+3=6 vs. (3+4=7 or 4+3=7), 3+3=6 vs. >7, and ≤3+4 vs. >3+4. Related to this, the logarithm link function was applied for parameters with skewed distribution. Both of these GEE methods were applied for the ADC median as well. To assess the added value of texture parameters to the ADC median in differentiating non-cancerous versus cancerous tissue and for differentiating between GS ≤3+4 vs. >3+4, bivariate GEE models were created for each texture feature with ADC median. Only those significant on univariate analyses were tested.

The Wald test p values from the regression model were reported. P-values ≤0.05 were considered statistically significant. All statistical analyses were performed using SAS 9.2 (SAS Institute Inc., NC, USA).

RESULTS

Of the 147 patients included in the analysis, 111 (75.5%) had one cancerous lesion ≥0.5ml on pathology, 33 patients (22.4%) had two and three patients (2.0%) had 3 cancerous lesions ≥0.5ml on pathology. Table 2 details the clinical and demographical data of the study population. Further analysis was done on a per-lesion basis, including 186 cancerous lesions ≥0.5ml on pathology, of which 143 (76.9%) were located in the PZ and 43 (23.1%) were in the TZ. The majority of the lesions were classified as Gleason score 3+4=7 (n=109, 58.6%), whereas 33 lesions (17.7%) had a Gleason score 6, 25 lesions (13.4%) had a Gleason score 4+3=7, and 19 lesions (10.2%) had a Gleason score ≥8.

Texture Features

Differentiation of cancerous and non-cancerous tissue in the PZ—Table 3 summarizes the means and standard deviations of the five texture features (Energy, Entropy, Correlation, Homogeneity, and Inertia) of 143 PZ cancers and non-cancerous PZ tissue on T2WI and the ADC maps. On both T2WI and ADC maps, Entropy and Inertia were significantly higher whereas Energy, Correlation, and Homogeneity were significantly lower in prostate cancer foci than in non-cancerous PZ tissue (p-values: <.0001–0.008).

Differentiation of cancerous and non-cancerous tissue in the TZ—Table 3 also summarizes the means and standard deviations of the five texture features of 43 TZ cancers and non-cancerous TZ tissue. On ADC maps, Entropy and Inertia were significantly higher in the cancer lesions whereas Energy, Correlation and Homogeneity were significantly lower than in non-cancerous TZ tissue (all p-values: <.0001). On T2-weigted images, Inertia was significantly higher in cancer lesions than in non-cancerous prostate tissue (p=0.001), whereas Correlation was significantly lower (p=0.041). There was no significant difference in Energy, Entropy and Homogeneity of cancer lesions and non-cancerous prostate tissue on T2WI.

Association between texture features and Prostate Cancer Gleason Score (GS)—Table 4 details the association of the GS of PZ prostate cancers (n=143) and the five texture parameters on T2WI and ADC maps. On the ADC maps, higher PZ GS was associated with higher Entropy (Figure 4A) and lower Energy (Figure 4B). None of the texture features of T2WI showed significant associations with GS for all three GS groupings. However, Homogeneity was found to significantly differentiate 3+3=6 vs. ≥8 and ≤3+4 vs. >3+4. Due to the small numbers of TZ cancers in each GS category, MRI texture and GS associations in TZ cancers were not evaluated.

Added value of texture features to the median ADC—The median ADC values of cancer lesions were significantly lower than the median ADC values of non-cancerous prostate tissue in the PZ (1061±203 vs. 1511±274, p<0.0001) and the TZ (1014±190 vs. 1407±208 10^{-6} mm^2/s, p<.0001), respectively. In PZ cancer lesions, the median ADC was negatively correlated with the lesion's GS (p<.0001, detailed numbers provided in Table 4). After adjusting for median ADC, Energy, Entropy, Correlation, and Homogeneity on the ADC map were independently associated with tumour presence (Table 5). For differentiating

GS ≤3+4 vs. ≥4+3, entropy measured on the ADC map remained significant even after controlling for the median ADC, (p=0.0291, Table 6).

DISCUSSION

In this study we found that Haralick texture features derived from T2-weighted images and ADC maps have the potential to differentiate between prostate cancer and non-cancerous prostate tissue. We also found that Entropy derived from the ADC map is significantly associated with prostate cancer Gleason score in the PZ, independently from the median ADC value. Haralick texture analysis may therefore contribute to prostate cancer detection and risk-stratification, without the need for acquiring additional MRI sequences. Although these findings are an encouraging initial step, additional efforts focusing on better understanding of the underlying biology that is being measured through texture analysis, as well as a better delineation of the incremental value of texture analysis compared to or in combination with other analytic approaches, are warranted.

Preliminary reports have hinted at the potential use of texture analysis in prostate cancer imaging. On transrectal ultrasound images, Huynen et al. found that with the combination of five Haralick texture features (among others Entropy and Inertia) they were able to prospectively discriminate non-cancerous from malignant prostate tissue in 30 patients with a sensitivity and specificity of 86% and 88%, respectively [29]. Another study evaluated a computer-assisted diagnosis system for peripheral zone prostate cancer detection in 20 patients and found that the Entropy on T2WI was one of the most discriminant features between non-cancerous and malignant tissue [21]. Another group found that, out of 110 T2-w MRI-derived variables, Haralick Entropy was one of the top 20 features to accurately identify peripheral zone prostate cancer in 22 patients [30]. There are no prior reports in the literature evaluating the use of Haralick texture parameters for assessing prostate cancer aggressiveness. Our study included data from a relatively large collective and both anatomical and functional MR imaging sequences. It provides the basis for the hypothesis that Haralick texture features of prostate MR images offer a possibility to retrieve additional information to that provided by the intrinsic parameters measured on each MR sequence (e.g. MR signal intensities on T2WI and ADC values on DW-MRI).

Our study has several limitations. First, it is a retrospective design as the MRI examinations were done as staging procedures for newly-diagnosed prostate cancer and were part of the patients' diagnostic workup, whereas texture analysis was retrospectively applied to existing data. To reduce the possibility of confirmation bias, the image segmentation and the calculation of the texture features were performed by different teams of investigators, and the computational scientists who calculated the texture features were blinded to the patients' clinical history and imaging and pathology findings. Second, only patients undergoing radical prostatectomy were included in the study in order to ensure the most accurate imaging to pathology correlation possible by using whole-mount step-section tumour maps as the standard of reference. This selection bias explains the relatively small number of Gleason Score 3+3 lesions in our cohort and may limit the generalizability of our results to patients in whom radical prostatectomy is not deemed a management option. Third, correlation between the MR images and the whole-mount step-section specimens may not

have been perfectly accurate as the use of an endorectal coil is known to potentially compress and deform the prostate gland and cancer lesions. We tried to minimize inaccuracies by a consensus approach of image segmentation but this issue remains a potential source of error. Fourth, MRI acquisition parameters were variable but textures, specifically the Haralick texture features, are computed using the relative values of pixel intensities between specific pixels. Differences in MR image acquisition will therefore not necessarily impact the texture computation. Fifth, this study was designed as a proof-of-concept analysis. It showed that Haralick texture analysis of prostate MRI yields meaningful results and therefore justifies more detailed investigations. However, our data cannot determine the incremental clinical value of this technique and prospective comparative studies are needed.

In summary, several Haralick based texture features showed significant differences between non-cancerous and malignant prostate tissue and in tumours with different Gleason scores. Additional work is necessary to evaluate the incremental value of Haralick texture over other quantitative metrics derived from multiparametric prostate MRI and to understand the underlying biology evaluated by texture analysis.

Acknowledgments

The scientific guarantor of this publication is Andreas Wibmer, MD. The authors of this manuscript declare no relationships with any companies, whose products or services may be related to the subject matter of the article. The authors state that this work has not received any funding. Junting Zheng, Debra Goldman and Chaya Moskowitz kindly provided statistical advice for this manuscript. All have significant statistical expertise. Institutional Review Board approval was obtained. Written informed consent was waived by the Institutional Review Board. No study subjects or cohorts have been previously reported. Methodology: retrospective, experimental, performed at one institution.

References

1. Gondo T, Hricak H, Sala E, et al. Multiparametric 3T MRI for the prediction of pathological downgrading after radical prostatectomy in patients with biopsy-proven Gleason score 3 + 4 prostate cancer. Eur Radiol. 2014; doi: 10.1007/s00330-014-3367-7
2. Salami SS, Vira MA, Turkbey B, et al. Multiparametric magnetic resonance imaging outperforms the Prostate Cancer Prevention Trial risk calculator in predicting clinically significant prostate cancer. Cancer. 2014; 120:2876–2882. [PubMed: 24917122]
3. Klotz L, Zhang L, Lam A, Nam R, Mamedov A, Loblaw A. Clinical results of long-term follow-up of a large, active surveillance cohort with localized prostate cancer. J Clin Oncol. 2010; 28:126–131. [PubMed: 19917860]
4. NICE. [Accessed 2015/01/31] Prostate cancer: diagnosis and treatment. 2014. Available via http://www.nice.org.uk/guidance/CG175
5. Heidenreich A, Bastian PJ, Bellmunt J, et al. EAU guidelines on prostate cancer. part 1: screening, diagnosis, and local treatment with curative intent-update 2013. Eur Urol. 2014; 65:124–137. doi: 110.1016/j.eururo.2013.1009.1046. Epub 2013 Oct 1016. [PubMed: 24207135]
6. NCCN. [Accessed 2015/01/31] NCCN Clinical Practice Guidelines in Oncology (NCCN Guidelines®) Prostate Cancer Version 1.2015. Available via http://www.nccn.org/professionals/physician_gls/pdf/prostate.pdf
7. Thrift AP, Whiteman DC. Can we really predict risk of cancer? Cancer Epidemiol. 2013; 37:349–352. [PubMed: 23643191]
8. Barentsz JO, Richenberg J, Clements R, et al. ESUR prostate MR guidelines 2012. Eur Radiol. 2012; 22:746–757. [PubMed: 22322308]

9. Wang L, Mazaheri Y, Zhang J, Ishill NM, Kuroiwa K, Hricak H. Assessment of biologic aggressiveness of prostate cancer: correlation of MR signal intensity with Gleason grade after radical prostatectomy. Radiology. 2008; 246:168–176. [PubMed: 18024440]
10. Hambrock T, Somford DM, Huisman HJ, et al. Relationship between apparent diffusion coefficients at 3.0-T MR imaging and Gleason grade in peripheral zone prostate cancer. Radiology. 2011; 259:453–461. [PubMed: 21502392]
11. deSouza NM, Riches SF, Vanas NJ, et al. Diffusion-weighted magnetic resonance imaging: a potential non-invasive marker of tumour aggressiveness in localized prostate cancer. Clin Radiol. 2008; 63:774–782. [PubMed: 18555035]
12. Mazaheri Y, Shukla-Dave A, Hricak H, et al. Prostate cancer: identification with combined diffusion-weighted MR imaging and 3D 1H MR spectroscopic imaging--correlation with pathologic findings. Radiology. 2008; 246:480–488. [PubMed: 18227542]
13. Jung SI, Donati OF, Vargas HA, Goldman D, Hricak H, Akin O. Transition zone prostate cancer: incremental value of diffusion-weighted endorectal MR imaging in tumor detection and assessment of aggressiveness. Radiology. 2013; 269:493–503. [PubMed: 23878284]
14. Vargas HA, Akin O, Franiel T, et al. Diffusion-weighted endorectal MR imaging at 3 T for prostate cancer: tumor detection and assessment of aggressiveness. Radiology. 2011; 259:775–784. [PubMed: 21436085]
15. Donati OF, Mazaheri Y, Afaq A, et al. Prostate Cancer Aggressiveness: Assessment with Whole-Lesion Histogram Analysis of the Apparent Diffusion Coefficient. Radiology. 2013; doi: 10.1148/radiol.13130973:130973
16. Peng Y, Jiang Y, Yang C, et al. Quantitative analysis of multiparametric prostate MR images: differentiation between prostate cancer and normal tissue and correlation with Gleason score--a computer-aided diagnosis development study. Radiology. 2013; 267:787–796. [PubMed: 23392430]
17. Coffey N, Schieda N, Cron G, Gulavita P, Mai KT, Flood TA. Multi-parametric (mp) MRI of prostatic ductal adenocarcinoma. J Magn Reson Imaging. 2014; 10:24694.
18. Donati OF, Mazaheri Y, Afaq A, et al. Prostate cancer aggressiveness: assessment with whole-lesion histogram analysis of the apparent diffusion coefficient. Radiology. 2014; 271:143–152. doi: 110.1148/radiol.13130973. Epub 13132013 Dec 13130912. [PubMed: 24475824]
19. Haralick RM. Statistical and Structural Approaches to Texture. Proceedings of the Ieee. 1979; 67:786–804.
20. Haralick RM, Shanmuga K, Dinstein I. Textural Features for Image Classification. Ieee Transactions on Systems Man and Cybernetics Smc. 1973; 3:610–621.
21. Niaf E, Rouviere O, Mege-Lechevallier F, Bratan F, Lartizien C. Computer-aided diagnosis of prostate cancer in the peripheral zone using multiparametric MRI. Phys Med Biol. 2012; 57:3833–3851. [PubMed: 22640958]
22. Lopes DFD, Ramalho GLB, de Medeiros FNS, Costa RCS, Araujo RTS. Combining features to improve oil spill classification in SAR images. Structural, Syntactic, and Statistical Pattern Recognition, Proceedings. 2006; 4109:928–936.
23. Conners RW, Trivedi MM, Harlow CA. Segmentation of a High-Resolution Urban Scene Using Texture Operators. Computer Vision Graphics and Image Processing. 1984; 25:273–310.
24. Oczeretko E, Borowska M, Kitlas A, Borusiewicz A, Sobolewska-Siemieniuk M. Fractal analysis of medical images in irregular regions of interest. IEEE Intl Conf on Bioinformatics and BioEngineering. 2008:1–6.
25. Tixier F, Le Rest CC, Hatt M, et al. Intratumor heterogeneity characterized by textural features on baseline 18F-FDG PET images predicts response to concomitant radiochemotherapy in esophageal cancer. J Nucl Med. 2011; 52:369–378. [PubMed: 21321270]
26. Tan S, Kligerman S, Chen W, et al. Spatial-temporal [(1)(8)F]FDG-PET features for predicting pathologic response of esophageal cancer to neoadjuvant chemoradiation therapy. Int J Radiat Oncol Biol Phys. 2013; 85:1375–1382. [PubMed: 23219566]
27. Yoo TS, Ackerman MJ, Lorensen WE, et al. Engineering and algorithm design for an image processing Api: a technical report on ITK--the Insight Toolkit. Stud Health Technol Inform. 2002; 85:586–592. [PubMed: 15458157]

28. Martin, K. Mastering CMake: A Cross-Platform Build System. Kitware Inc; 2003.
29. Huynen AL, Giesen RJB, Delarosette JJMCH, Aarnink RG, Debruyne FMJ, Wijkstra H. Analysis of Ultrasonographic Prostate Images for the Detection of Prostatic-Carcinoma - the Automated Urologic Diagnostic Expert-System. Ultrasound in Medicine and Biology. 1994; 20:1–10. [PubMed: 8197622]
30. Viswanath SE, Bloch NB, Chappelow JC, et al. Central gland and peripheral zone prostate tumors have significantly different quantitative imaging signatures on 3 tesla endorectal, in vivo T2-weighted MR imagery. Journal of Magnetic Resonance Imaging. 2012; 36:213–224. [PubMed: 22337003]

Key Points

1. Several Haralick texture features may differentiate non-cancerous and cancerous prostate tissue.
2. Tumour Energy and Entropy on ADC maps correlate with Gleason score.
3. T2w-images-derived texture features are not associated with the Gleason score.

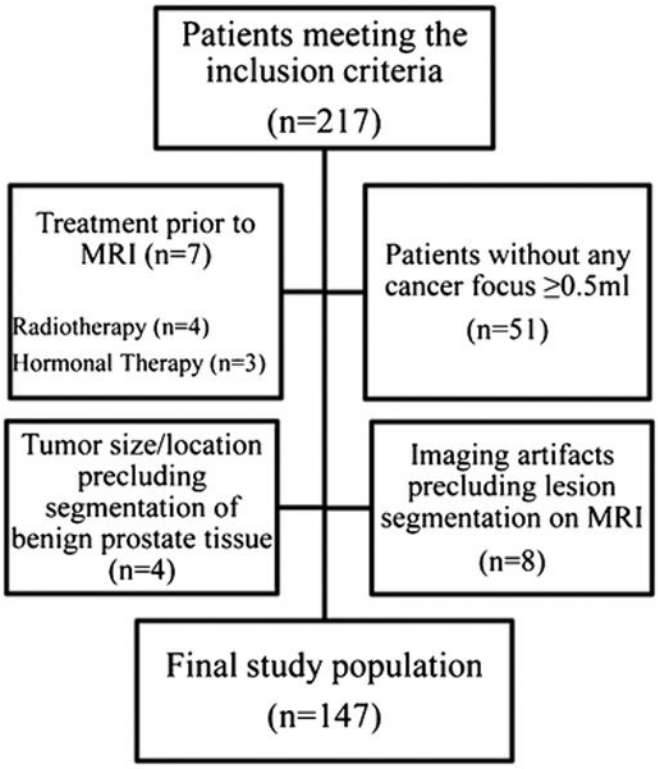

Figure 1.
Flowchart of patient selection

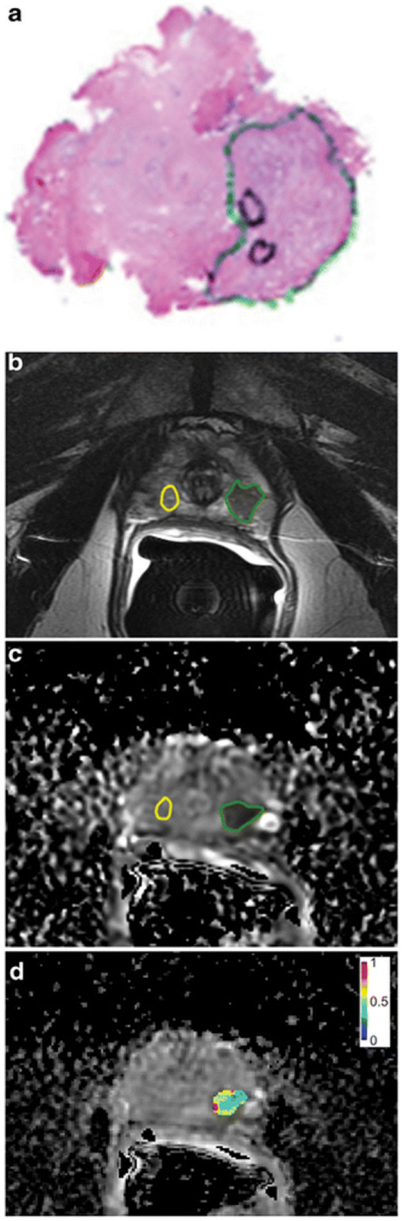

Figure 2.

63-year-old man with Gleason 3+4 prostate cancer demonstrated on the whole-mount prostatectomy pathology map (a). Using this as reference, the tumour was identified and a region of interest placed (green line) on the T2-weighted images (b) and ADC map (c). An area of benign prostatic tissue was also outlined on the same sequences (yellow line).

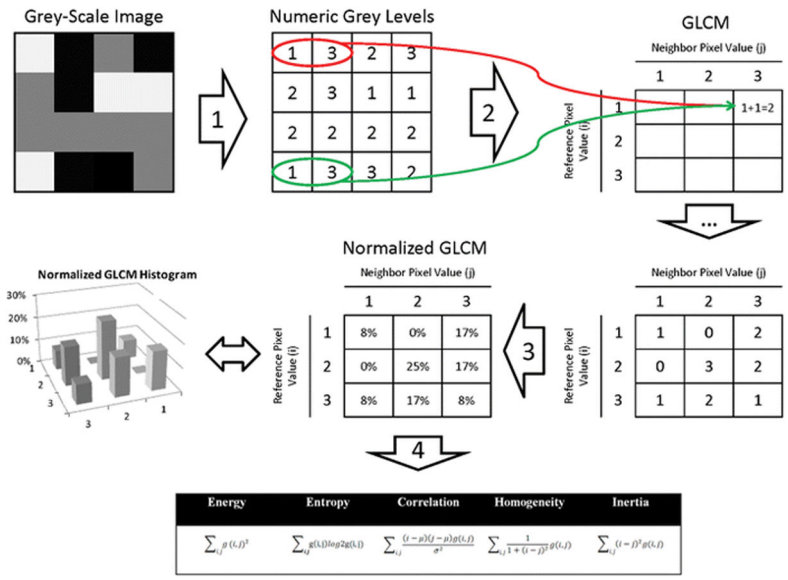

Figure 3.

Explanation of the calculation of texture features from a grey-level co-occurrence matrix (GLCM). For simplicity, a 4 × 4 pixel grey-scale image with only three grey-levels (i.e. light-grey [≡1], dark-grey [≡2], and black [≡3]) was chosen. In **Step 1**, the grey-scale image is transcribed to a corresponding grid of numeric grey-levels. A GLCM is deducted from this grid by considering the relationship of every pixel to its neighbourhood. For this example, a ‘neighbour pixel’ was defined as one that is located immediately to the right of each ‘reference pixel’. We start with the light-grey [≡1] pixel in the left-upper corner. It’s ‘neighbour’ is a black [≡3] pixel, meaning that a light-grey [≡1] and black [≡3] pixel ‘co-occurred’, as indicated by the red circle in the diagram. There is one other co-occurrence of light-grey [≡1] and black [≡3] in the diagram (highlighted by a green circle). In **Step 2**, the count of all possible co-occurrences is recorded in a table, which - after its completion - is named the GLCM. In **Step 3**, the GLCM is normalized so that each cell doesn’t contain a count of every possible co-occurrence but its probability. These probabilities provide the basis for the calculation of the various texture features according to the equations shown (**Step 4**). In a ‘real-world’ application of this principle, ‘neighbourhood’ can be defined in various ways by changing the directions and distances between ‘reference pixels’ and ‘neighbour pixels’.

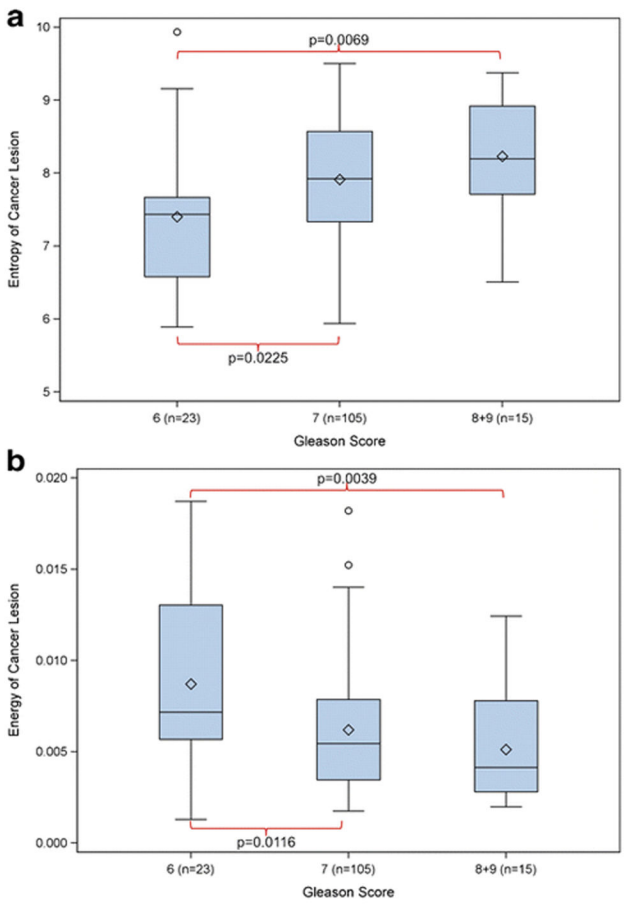

Figure 4.

Box-and-Whisker plots displaying the distribution of Haralick Entropy (A) and Energy (B) of peripheral zone prostate cancer lesions (n=143) on ADC maps, stratified by the lesions' Gleason scores (3+3=6, 3+4=7 or 4+3=7, and >7). The detailed numbers and p-values are provided in Table 4.

Table 1

Description of the five Haralick texture features used in this study

Texture Feature	Description
Energy	Computed as the average of the gray level co-occurrences, it captures the extent of similarity of voxels in a given region.
Entropy	Captures the amount of variation in the co-occurrence of the different voxels and is a measure of disorder in the distribution of signal intensities.
Correlation	Captures how the pairs of voxels are correlated to other voxel pairs as positive, zero, or negative correlation.
Homogeneity (Difference Moment)	Computes the homogeneity of the co-occurrence pairs.
Inertia (Contrast)	Computes the amount of dissimilarity of the co-occurrence pairs and is a measure of variation in signal intensities.

Table 2

Patient characteristics (n=147)

	Mean ± SD, Median (Range)
Age at Prostatectomy (years)	59.0±7.5 58.9 (38.0–75.2)
Time from MRI to prostatectomy (days)	22.3±21.5 15 (1–100)
Serum PSA (ng/ml)	7.2±7.5 5.5 (1.1–60.9)
	N (%)
Prostatectomy Gleason Score	
3+3=6	33 (17.7)
3+4=7	109 (58.6)
4+3=7	25 (13.4)
≥8	19 (10.2)
Number of cancer lesions ≥0.5ml on histopathology	
Number of patients with1 lesion	111 (75.5)
Number of patients with 2 lesions	33 (22.4)
Number of patients with 3 lesions	3 (2.0)

PSA: prostate-specific antigen; SD: standard deviation

Table 3

Texture features of cancerous and non-cancerous prostate tissue

Peripheral Zone						
Texture feature	**T2-weighted images**			**ADC map**		
	Cancer lesion	**Non- cancerous tissue**	**p- value**	**Cancer lesion**	**Non- cancerous tissue**	**p-value**
Energy	0.028 ± 0.032	0.039 ± 0.04	0.008	0.006 ± 0.004	0.032 ± 0.026	<.0001
Entropy	6.34 ± 1.33	5.58 ± 1.22	<.0001	7.86 ± 0.88	5.42 ± 0.8	<.0001
Correlation	0.083 ± 0.106	0.17 ± 0.21	<.0001	0.009 ± 0.009	0.055 ± 0.049	<.0001
Homogeneity	0.43 ± 0.13	0.49 ± 0.15	<.0001	0.21 ± 0.05	0.33 ± 0.09	<.0001
Inertia	14.02 ± 20.31	6.62 ± 10.26	<.0001	67.01 ± 54.32	14.04 ± 23.98	<.0001

Transition Zone						
Texture feature	**T2-weighted images**			**ADC map**		
	Cancer lesion	**Non- cancerous tissue**	**p-value**	**Cancer lesion**	**Non- cancerous tissue**	**p-value**
Energy	0.068 ± 0.06	0.08 ± 0.098	0.413	0.007 ± 0.004	0.016 ± 0.006	<.0001
Entropy	5.1 ± 1.55	4.72 ± 1.53	0.069	7.78 ± 0.85	6.29 ± 0.55	<.0001
Correlation	0.23 ± 0.28	0.41 ± 0.56	0.041	0.009 ± 0.008	0.029 ± 0.023	<.0001
Homogeneity	0.55 ± 0.15	0.59 ± 0.19	0.141	0.21 ± 0.06	0.27 ± 0.09	<.0001
Inertia	5.28 ± 6.44	2.71 ± 3.22	0.001	59.17 ± 53.4	19.9 ± 14.35	<.0001

Data are presented as means ± standard deviation. The difference of parameter values between tumor and non-cancerous tissue was calculated and tested using the generalized estimating equations (GEE) method with a robust covariance matrix and independent correlation structure to take into account multiple tissue samples per patients.

Table 4

Association between Haralick texture features and peripheral zone prostate cancer Gleason score.

	T2-Weighted Images				**comparison p values**		
	3+3=6	**3+4=7**	**4+3=7**	**>7**	**3+3=6 vs (3+4=7 or 4+3=7)**	**3+3=6 vs >7**	**≤3+4=7 vs. >3+4=7**
Energy	0.029 ± 0.019	0.026 ± 0.031	0.023 ± 0.029	0.047 ± 0.05	0.40	0.10	0.38
Entropy	5.96 ± 1.03	6.49 ± 1.38	6.68 ± 1.31	5.56 ± 1.22	0.0234	0.29	0.64
Correlation	0.083 ± 0.08	0.071 ± 0.079	0.081 ± 0.15	0.15 ± 0.16	0.76	0.10	0.15
Homogeneity	0.42 ± 0.1	0.41 ± 0.13	0.43 ± 0.14	0.55 ± 0.11	0.86	0.0004	0.0012
Inertia	9.06 ± 7.28	16.58 ± 23.36	16 ± 21.98	4.65 ± 3.49	0.012	0.0096	0.08
	ADC Map				**comparison p values**		
	3+3=6	**3+4=7**	**4+3=7**	**>7**	**3+3=6 vs (3+4=7 or 4+3=7)**	**3+3=6 vs >7**	**≤3+4 =7 vs. >3+4=7**
Energy	0.009 ± 0.005	0.006 ± 0.003	0.006 ± 0.004	0.005 ± 0.003	0.0116	0.0039	0.0102
Entropy	7.4 ± 1.04	7.84 ± 0.78	8.14 ± 0.9	8.23 ± 0.8	0.0225	0.0069	0.0019
Correlation	0.007 ± 0.009	0.01 ± 0.01	0.011 ± 0.007	0.008 ± 0.007	0.07	0.63	0.39
Homogeneity	0.19 ± 0.06	0.2 ± 0.05	0.23 ± 0.05	0.2 ± 0.05	0.11	0.61	0.12
Inertia	73.91 ± 51.96	66.13 ± 58.14	54.92 ± 36.57	81.27 ± 61.31	0.28	0.70	0.76
ADC Median (10^{-6} mm^2/s)	1186.78 ± 215.68	1081.65 ± 198.26	955.4 ± 160.44	936.27 ± 123.32	0.0004	<.0001	<.0001

Data are presented as mean ± standard deviation. A generalized linear regression and the generalized estimating equations (GEE) method were used to examine the association between each texture parameter and tumour Gleason score. Logarithm link function was applied for parameters with skewed distribution (i.e.: Energy, Correlation, and Inertia). The Wald test p values from the regression model were reported for each parameter.

Table 5

Bivariate models for the differentiation of cancerous vs. non-cancerous prostate tissue on ADC maps with texture parameters adjusted for median ADC. Significant p-values indicate that the respective texture feature was independently associated with the presence of cancerous tissue.

	Texture Feature			Median ADC Value**		
	Odds Ratio	**95% CI**	**p-value**	**Odds Ratio**	**95% CI**	**p-value**
*Energy**	1.67	[1.38–2.02]	**<.0001**	2.77	[1.90–4.05]	**<.0001**
Entropy	0.02	[0.00–0.09]	**<.0001**	2.76	[1.91–4.00]	**<.0001**
*Correlation**	1.13	[1.06–1.19]	**<.0001**	2.36	[1.83–3.04]	**<.0001**
*Homogeneity**	1.02	[1.02–1.03]	**<.0001**	2.52	[1.93–3.28]	**<.0001**
Inertia	0.93	[0.87–1.01]	0.07	2.43	[1.75–3.38]	**<.0001**

* OR in units of 1000.

** OR in units of 1/100,

CI: confidence interval

Table 6

Bivariate models for the differentiation of Gleason score ≤3+4 vs. >3+4 on ADC maps with texture parameters adjusted for median ADC. Texture parameters that were significantly correlated to the Gleason score on multivariate analysis (i.e. Energy and Entropy) were included. Significant p-values indicate that the respective texture feature was independently associated with the Gleason score.

	Texture Feature			ADC Value**		
	Odds Ratio	**95% CI**	**p-value**	**Odds Ratio**	**95% CI**	**p-value**
*Energy**	0.92	[0.82–1.04]	0.20	0.63	[0.51–0.79]	**<.0001**
Entropy	1.74	[1.06–2.86]	**0.0291**	0.64	[0.51–0.79]	**<.0001**

* OR in units of 1000.

** OR in units of 1/100,

CI: confidence interval